A Framework to Assess the Seismic Performance of Multiblock Tower Structures as Gravity Energy Storage Systems

José E. Andrade, M.ASCE[1]; Ares J. Rosakis, M.ASCE[2]; Joel P. Conte, M.ASCE[3];
José I. Restrepo, M.ASCE[4]; Vahe Gabuchian[5]; John M. Harmon[6];
Andrés Rodriguez[7]; Arpit Nema[8]; and Andrea R. Pedretti[9]

Abstract: This paper proposes a framework for seismic performance assessment of mutiblock tower structures designed to store renewable energy. To perform our assessment, we deployed, in tandem, physical and numerical models that were developed using appropriate scaling for Newtonian systems that interact via frictional contact. The approach is novel, breaking away from continuum structures for which Cauchy scaling and continuum mechanics are used to model systems. We show that our discontinuous approach is predictive and consistent. We demonstrate predictiveness by showing that the numerical models can reproduce with high fidelity the physical models deployed across two different scales. Consistency is demonstrated by showing that our models can be seamlessly compared across scales and without regard for whether the model is physical or numerical. The integrated theoretical-numerical-experimental approach provides a robust framework to study multiblock tower structures, and the results of our seismic performance assessments are promising. These findings may open the door for new analysis tools in structural mechanics, particularly those applied to gravity energy storage systems. **DOI: [10.1061/(ASCE)EM.1943-7889.0002159](#).** © 2022 American Society of Civil Engineers.

Introduction

The world population is expected to reach 10 billion by 2050, necessitating a corresponding increase of 200% in energy output (UN 2019). At the same time, the United States and other nations have goals to reduce CO_2 levels by 80% by 2050 (Markolf et al. 2020). To achieve these massive goals, green energies, such as solar and wind, are being aggressively pursued to increase the amount of energy available without the negative impact of CO_2 production. The intermittent nature of solar and wind power production, peaks in demand, and the need for resilient infrastructure have created the need for large-scale energy storage (Loveless 2012). As of 2019, the United States produced 4×10^9 MWh of electricity, with only 431 MWh of energy storage available, a gap of 7 orders of magnitude (EIA 2020; Zablocki 2019). It is estimated that the United States will require 266 GW of storage for the electric grid by 2030, up from 176.5 GW in 2017 (IEA 2017). This number is expected to increase to 942 GW by 2040, requiring an investment in energy storage of $620 billion over the next two decades (Henze 2018).

Today, electricity storage is dominated by pumped storage hydropower (PSH), furnishing 95% of the large-scale storage (EERE 2021). One of the appeals of PSH is simplicity: the idea is to use gravity to store energy in an uphill water reservoir when energy is produced, and then release it to a downstream reservoir, converting potential energy into kinetic energy in the process. On the other hand, PSH is limited by topography: there are only so many places on earth where upstream-downstream reservoir systems can be built. There is clearly a need to find alternative energy storage systems that share the simplicity of PSH but avoid its limitations. One potentially revolutionary gravity-driven system is being introduced by Energy Vault, Inc. (EV). Fig. 1 shows EV's entirely novel energy storage concept, which was recently proposed and is currently being demonstrated in Arbedo-Castione, Switzerland. The proposed idea is to deploy relatively tall prototype (height, $\ell^P \approx 160$ m) multiblock tower structures (MTS) connected to renewable energy sources (e.g., solar, wind), using discrete blocks to store energy in the form of potential energy by lifting the blocks to accrue energy, just as in PSH. Thousands of blocks can be stacked up, as shown in Fig. 1(b), each block storing packets of energy that can then be consumed when needed.

The simplicity and promise of the MTS is remarkable, allowing up to 35 MWh of storage per tower anywhere in the world. The blocks are manufactured using a soil-cement mixture plus other

[1]Professor, Mechanical and Civil Engineering, California Institute of Technology, 1200 E California Blvd., Pasadena, CA 91125 (corresponding author). Email: jandrade@caltech.edu

[2]Professor, Graduate Aerospace Laboratories, California Institute of Technology, 1200 E California Blvd., Pasadena, CA 91125. Email: arosakis@caltech.edu

[3]Professor, Dept. of Structural Engineering, Univ. of California, San Diego 9500 Gilman Dr., La Jolla, CA 92093. Email: jpconte@ucsd.edu

[4]Professor, Dept. of Structural Engineering, Univ. of California, San Diego 9500 Gilman Dr., La Jolla, CA 92093. Email: jrestrepo@ucsd.edu

[5]Researcher, Graduate Aerospace Laboratories, California Institute of Technology, 1200 E California Blvd., Pasadena, CA 91125. Email: gabuchian@caltech.edu

[6]Graduate Student, Mechanical and Civil Engineering, California Institute of Technology, 1200 E California Blvd., Pasadena, CA 91125. Email: jhharmon@caltech.edu

[7]Graduate Student, Dept. of Structural Engineering, Univ. of California, San Diego 9500 Gilman Dr., La Jolla, CA 92093. Email: a1rodrig@eng.ucsd.edu

[8]Postdoctoral Researcher, Pacific Earthquake Engineering Research Center, Univ. of California, Berkeley 1301 S. 46th St., Richmond, CA 94804-4698. Email: anema@berkeley.edu

[9]Chief Technology Officer, Energy Vault, Inc., 4360 Park Terrace Dr., Westlake Village, CA 91361. Email: Andrea@energyvault.com
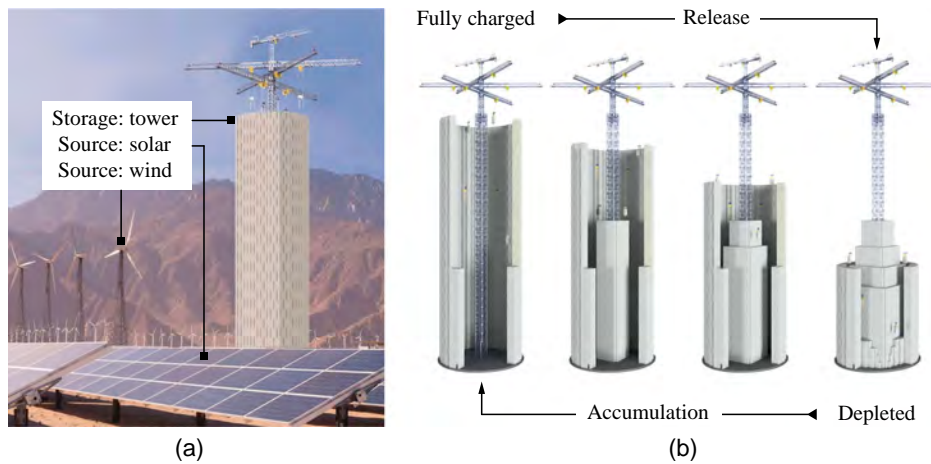
Fig. 1. Energy Vault's gravity energy storage system concept: (a) MTS proposed to store renewable energy shown conceptually to be close to green energy sources; and (b) energy storage mechanisms for charging and discharging energy using MTS. An autonomous six-arm crane is used to move blocks as the tower charges and discharges. In our seismic performance assessment, we focused on the fully charged configuration shown on the far left. (Images courtesy of Energy Vault, Inc.)

materials from construction/demolition debris and have a prescribed weight. From a structural mechanics perspective, the novel MTS concept introduces interesting questions that need to be explored: How can we model such discontinuous structures both physically and numerically? What are the governing scaling laws that can be used to appropriately design and deploy physical models across different scales? Particularly relevant is the structural seismic performance of MTS.

In this paper, we take a first step at answering these questions by presenting the results of a year-long campaign to assess the seismic performance of MTS. We deployed numerical and physical models in tandem, all against the backdrop of newly derived scaling laws to achieve not only accurate modeling but also consistency. Here, we define consistency as the ability to compare physical and virtual models across scales and material properties. This integrated theoretical-numerical-experimental approach was adopted deliberately, since the novel MTS break away from conventional continuum structures for which Cauchy scaling and continuum mechanics provide the theoretical backbone to model and analyze such systems. Instead, MTS are discontinuous, with discrete blocks serving as the basic fundamental unit. The discontinuous nature of MTS necessitated a discrete approach to modeling and analysis, thus requiring a new theoretical backbone fundamentally based on Newtonian mechanics. The preferred modeling and analysis approach is therefore the discrete element method (DEM) in which each block can be simulated as an individual rigid unit whose interactions are controlled by Newton's laws and basic frictional contact mechanics. The numerical models needed complementary physical models at various scales to be properly validated. At the same time, proper scaling for frictional, multiblock, gravity-driven systems was necessary to design experiments that are representative of the prototype, are useful for validation, and can be consistently compared.

This paper is the result of a team effort between California Institute of Technology (Caltech), University of California San Diego, University of California Berkeley (UCB), and EV and is structured as follows. We first present the modeling campaign methodology to assess the seismic performance of MTS, with physical and numerical modeling intertwined by proper scaling. The physical modeling campaign was deployed using shake tables across two different scales: a tabletop scale (1:107) at Caltech and an engineering scale (1:25) at UCB. To appropriately scale from the

field prototype to these two modeling scales, we present our scaling methodology with a key resulting dimensionless number μ^N (Rosakis et al. 2021) appropriate for such gravitational-frictional systems. We then present the numerical models, which are furnished using the level set discrete element method (LS-DEM) (Kawamoto et al. 2016). We focus on the novel features of LS-DEM, including the process to capture a block's morphology as well as the material parameter's values used in our predictions. At the heart of this paper, we compare the results of the physical and numerical models, which serves as validation of our theoretical approach to obtain μ^N and associated similitude law, as well as validation of our novel numerical models developed using LS-DEM. We are pleased to report that the results are encouraging, showing remarkable predictive capabilities of the LS-DEM models as well as robust consistency across scales and models. Finally, we close the paper with some discussion on our findings and their significance for gravity-driven storage of renewable energy.

Methodology: Similitude and Physical and Numerical Modeling

The main goal of our campaign is to validate the computational (virtual) models of EV's MTS using appropriate physical models across scales, as shown in Fig. 2. To this end, two major tasks need to be undertaken: (1) development of appropriate physical models ($M_{1,2}$) of MTS at various scales; and (2) development of virtual models ($V_{1,2}$) of MTS. Direct comparison with the prototype is not yet feasible; there are no full-scale operational MTS at this time, hence the importance and relevance of appropriate physical models to enable comparisons, i.e., V_1 versus M_1 and V_2 versus M_1. We adopt the definition of physical model given by Janney et al. (1970): "A structural model is any structural element or assembly of structural elements built to a reduced scale (in comparison with full size structures) which is to be tested, and for which laws of similitude must be employed to interpret test results." To be feasible and effective, physical models are scaled relative to the prototype. This scaling requires an immediate choice of geometry, material, and loading (e.g., input ground motion record) for the physical model, hinging crucially on similitude. At the same time, similitude requirements are furnished by the derivation of dimensionless numbers (i.e., Π groups), which can be shown to control the physical system regardless of choice of basic dimensions, e.g., length,
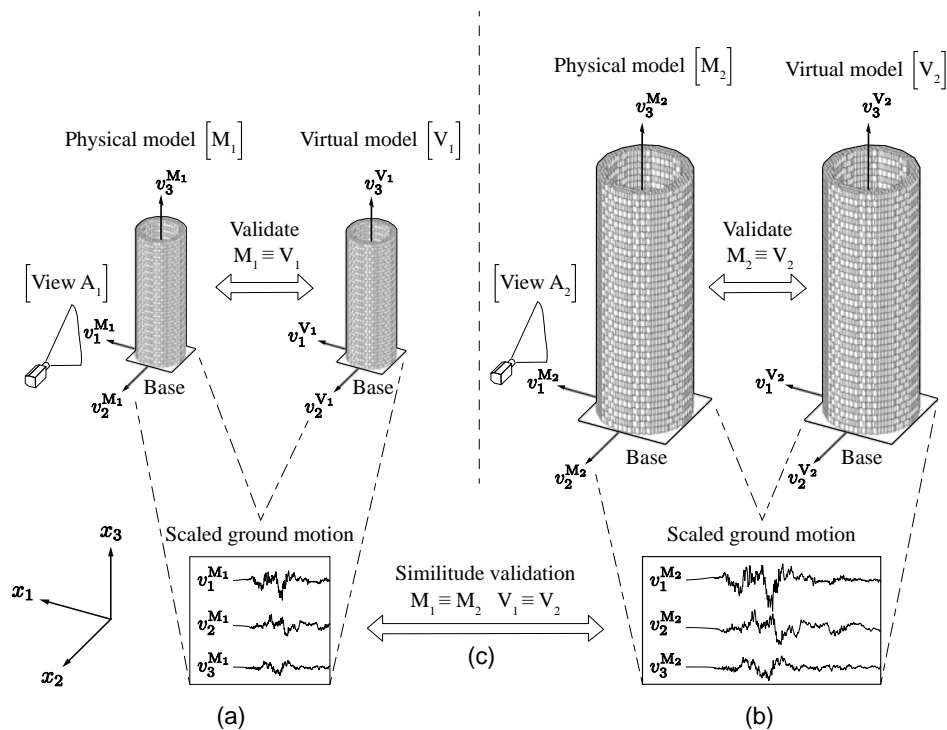
Fig. 2. Schematic representation of combined theoretical-physical-numerical modeling campaign deployed for MTS. Physical dynamic models were compared with virtual models of MTS: (a) validation at 1:107 scale comparing physical dynamic model M_1 to virtual LS-DEM model V_1; (b) validation at 1:25 scale comparing physical dynamic model M_2 to virtual LS-DEM model V_2; and (c) appropriately scaled input ground motions, achieved by imposing similitude requirements.

time, and mass. The choice of dimensionless numbers, which is the subject of an accompanying paper (Rosakis et al. 2021), drives the design of the physical models and the applied dynamic loading.

We designed and constructed the physical models as defined in Harris and Sabnis (1999): geometrically similar to the prototype in all respects, including the dynamic loads, furnished by shaking tables. As shown in Fig. 2, two physical modeling campaigns were devised and conducted: one at Caltech at 1:107, and another at UCB at 1:25. Below, we present some of the details of such direct dynamic models and how we achieved similitude across these different scales. Suffice it to say, using the Buckingham's pi theorem (BPT), we obtained Π groups, required to be invariant between prototype and model (Rosakis et al. 2021). These Π groups are specifically crafted to allow similitude between materials of different friction coefficients. One such Π group is $\Pi_1 := \mu^N$, a nondimensional number as mentioned above and defined in the section "Physical Modeling," where we provide an overview of its derivation. It turns out that μ^N is similar to the well-known Froude number F_r^N. Incidentally, for dynamic similitude of civil engineering structures, the most commonly used nondimensional numbers are the Cauchy number C^N, used when elasticity controls the response behavior of the system; and the Froude number F_r^N, used for appropriately scaling hydraulic and frictionless structural systems where gravitational loading is important (Moncarz and Krawinkler 1981). To our knowledge, no nondimensional number has been previously proposed to properly scale the dynamic behavior of multi-block systems whose nonlinear dynamic response is controlled by gravitational and frictional restoring forces.

Armed with μ^N to properly scale our MTS dynamic (physical) models, we designed a combined theoretical-numerical-experimental campaign whose methodology and key results we present in this paper. Fig. 3 shows an overview of the campaign, including the

physical models (specimens) developed, as well as the virtual models deployed. It is important to highlight that this was a unique exercise in which theory and modeling were deployed in tandem to analyze the MTS. The numerical models were deployed first, since these could readily explore ideas for theory and experiment. However, it was not until the theory and physical models came about that a deep understanding and validation of the numerical model were achieved. Below, we describe our efforts in validating the numerical models, and in the process, we describe the multiscale physical modeling campaign and then the intricacies of the numerical model used. Much like the theory and physical models, the numerical model had to represent the MTS accurately: capturing the block geometry, simulating the frictional contact interfaces, properly transmitting dynamical loading, and scaling to the thousands of blocks involved in the virtual and physical models. As shown in Fig. 3, complete consistency was imposed across all models, making it possible to compare M_1 with V_1, M_2 with V_2, but also, and most importantly, being able to analyze all results across models $M_{1,2}$ and $V_{1,2}$ consistently. The virtual model also enables us to show consistency: comparing the correctness of the similitude theory at levels of accuracy that are superior to the physical models. In what follows, we describe in detail the development of physical and virtual models for MTS, as well as the most salient results obtained with such consistent models.

Physical Modeling

The physical models developed herein are needed to experimentally study the nonlinear behavior of MTS subjected to input ground motions. The purpose of such experiments is the validation of our newly developed virtual models, to be presented in the next subsection. To be useful, a physical model should be able to predict
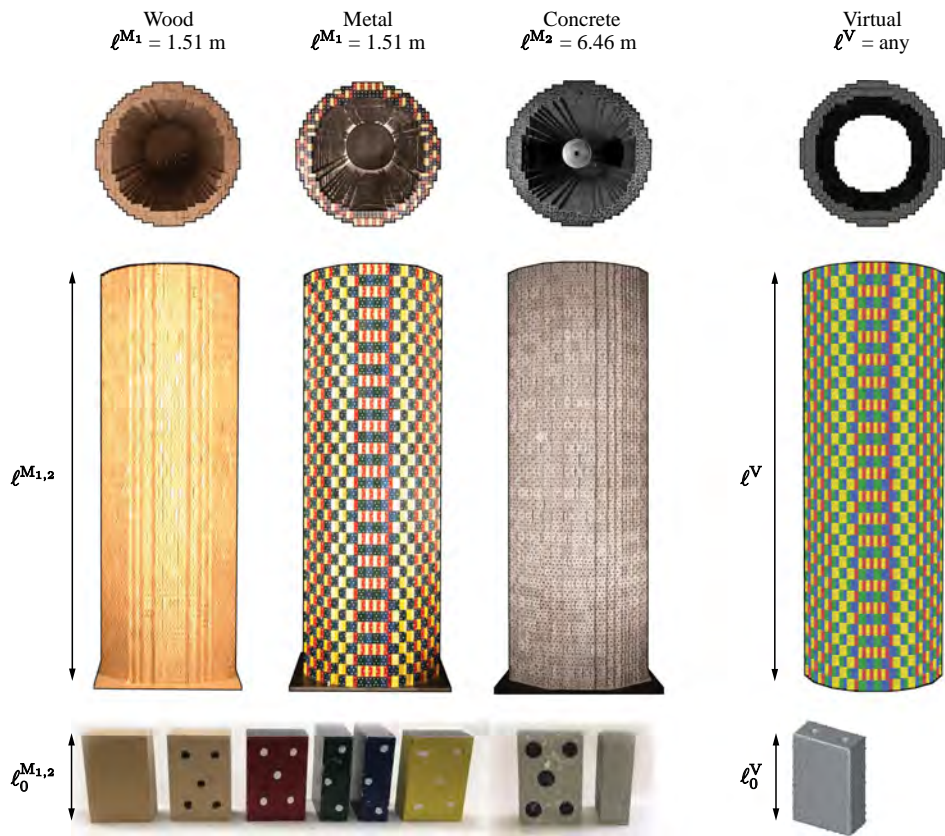
Fig. 3. Overview of experimental campaign showing physical models used with different geometries and materials (e.g., wood, metal, concrete). Virtual models were set up block by block with the same geometric and material properties, enabling direct comparison. The bottom row shows blocks as fundamental units of MTS. Note that physical blocks were marked to enhance kinematics tracking via DIC. Bottom right shows details of the virtual block, which is defined using level sets, requiring a grid of points where the level set function is defined. Validation necessitates complete consistency between all models, physical and virtual. Every tower consists of 38 stories or layers with 188 blocks each, for a total of 7,144 blocks. The pattern of each layer is shown in the top view (top row), with each layer alternating the pattern by 90°.

the nonlinear dynamic response of the MTS prototype. This necessitates similitude across scales, materials, loading, and instrumentation (diagnostics). In this section, we explain how we achieve similitude—and hence predictiveness—in our physical models. We focus on dynamic modeling theory (DMT), encompassing similitude requirements, geometric and material properties, and dynamic loads. We also explain our approach to multiscale model construction and diagnostics.

Our starting point is dynamic modeling theory (Moncarz and Krawinkler 1981). Perhaps the most fundamental component of DMT is dimensional analysis, which is built around BPT (Buckingham 1914) and the concept of similitude. The dynamic behavior of a physical system, such as the MTS we are interested in, can be said to be controlled by a dimensionally homogeneous function such that

$$f(v; a; \ell; \mu g; \rho) = 0 \qquad (1)$$

where the arguments of the (implicit) function f are physical quantities believed to be relevant to the MTS behavior. In the case of MTS systems, we assume the towers are composed of rigid blocks whose behavior is controlled by Newtonian mechanics and frictional contact restoring forces, with five main physical quantities of interest. The quantities of interest take the form of physical variables such as velocity v and acceleration a, geometrical parameters such as height of the tower ℓ (Fig. 3), material system parameters such as friction coefficient μ and mass density

ρ, and gravitational acceleration g. We point out that Eq. (1) is a modeling choice, as is usual in the application of BPT. This modeling carries the implicit assumption that sliding rather than rocking is the primary mode of deformation and that inertial effects on normal forces between interfaces are negligible compared with the weight. The validity of this assumption was checked by dynamic measurements of rocking angles, which were found to be minimal in our systems (see Appendix). At the same time, there are three basic units in these systems: length, time, and mass.

The BPT states that the dimensional homogeneous function f can be rewritten as a nondimensionally homogeneous function with two nondimensional variables, or Π groups, so that

$$F(\Pi_1; \Pi_2) = 0 \qquad (2)$$

where in this case, $\Pi_1 := \mu^N = v/\sqrt{\ell \mu g} = F_r^N/\sqrt{\mu}$ and $\Pi_2 := a/\mu g$. We note that $F_r^N := v/\sqrt{\ell g}$ is known as the Froude number, a typical dimensionless group used in frictionless gravity-controlled systems. The presence of the interblock friction coefficient μ next to the gravitational acceleration g in the denominator of both Π groups highlights the frictional-gravitational nature of the MTS (Rosakis et al. 2021). Similitude requires invariance in Π groups across scales in general and in particular between model (M) and the prototype (P) so that $\Pi_1^M = \Pi_1^P$ and $\Pi_2^M = \Pi_2^P$. Hence, according to DMT, two systems or models are similar if their Π groups are equal. Interestingly, for rigid-block systems, the material density does not appear in the Π groups and consequently is

not a physical variable, as will be corroborated experimentally (V. Gabuchian, A. Rosakis, J. Harmon, J. Andrade, J. Conte, and J. Restrepo, "Scaled experiments of multiblock tower structures I: Tabletop scale," submitted to Earthquake Eng. Struct. Dyn.). Further, one can choose three scales in this problem. We choose (for modeling convenience) the following scales between model (M) and prototype (P): the length scale $\lambda_\ell := \ell^M/\ell^P$, the gravity scale $\lambda_g := g^M/g^P$, and the frictional scale $\lambda_\mu := \mu^M/\mu^P$. In the modeling results presented herein, we chose $\lambda_\ell = \{1/107, 1/25\}$, $\lambda_g = 1$ and $\lambda_\mu \approx 1$. The former correspond to the length scales used in the lab at Caltech and UCB, respectively. The latter two correspond to the same gravitational field and similar coefficient of friction in the materials used for the unit blocks shown in Fig. 3. Finally, it then follows that the kinematic variables scale such that

$$v^M = v^P\sqrt{\lambda_\ell \lambda_\mu \lambda_g} \approx v^P\sqrt{\lambda_\ell}$$
$$a^M = a^P\lambda_\mu\lambda_g \approx a^P$$
$$t^M = t^P\sqrt{\frac{\lambda_\ell}{\lambda_\mu\lambda_g}} \approx t^P\sqrt{\lambda_\ell} \tag{3}$$

since $\lambda_\mu\lambda_g \approx 1$ for the results presented herein. These scaling relations were used in the construction, excitation, and instrumentation of the experiments conducted at the tabletop and engineering scales, described next.

Tabletop Scale Models ($\lambda_l = 1/107$)

This set of experiments was performed at Caltech. The details of this portion of the physical modeling campaign are specified in an upcoming publication (V. Gabuchian, A. Rosakis, J. Harmon, J. Andrade, J. Conte, and J. Restrepo, "Scaled experiments of multiblock tower structures I: Tabletop scale," submitted to Earthquake Eng. Struct. Dyn.). Fig. 4(a) shows a detailed picture of the experimental layout at this scale. The main dimension of the tower is $\ell^{M_1} = 1.51$ m [Fig. 4(a)], with corresponding basic block dimensions of $\ell_0^{M_1} = 4$ cm (Fig. 3). The blocks used were made out of wood and metal (aluminum). In this paper, we focus exclusively on the wood towers and will report the results on the metal tower in a future publication (V. Gabuchian, A. Rosakis, J. Harmon, J. Andrade, J. Conte, and J. Restrepo, "Scaled experiments of multiblock tower structures I: Tabletop scale," submitted to Earthquake Eng. Struct. Dyn.). Unlike the aluminum blocks, wood blocks have friction coefficients similar to those of concrete as shown in Table 2 and hence $\lambda_\mu \approx 1$, and the experiments were conducted under full gravitational acceleration, i.e., $\lambda_g = 1$. Hence, the only major difference between the models and prototype is the length scaling λ_ℓ.

In this paper, we showcase the results of a test on a wood tower that experiences the 2019 $M_w = 7.1$ Ridgecrest earthquake shown in Table 1 because of its relevant location to solar and wind farms in California. We simulated the velocity time history of the strong motion as recorded at China Lake station 3.5 km away from the
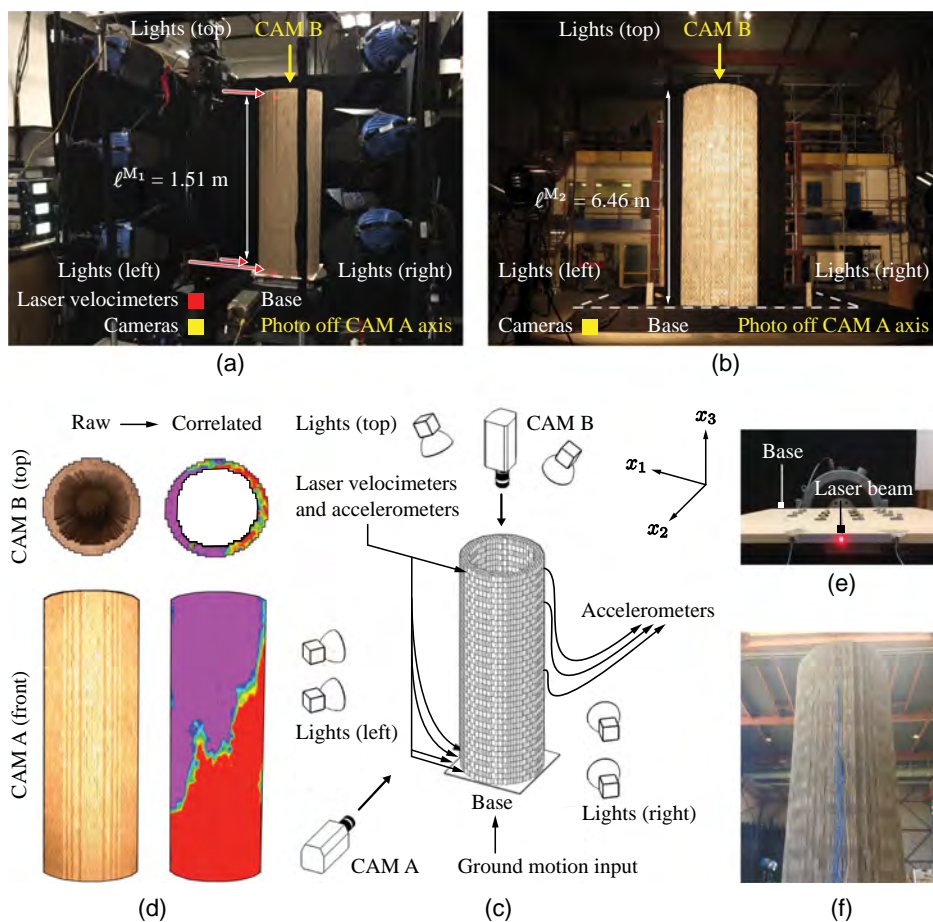
Fig. 4. General layout of physical models: (a) Caltech ($\lambda_\ell = 1/107$); and (b) UCB ($\lambda_\ell = 1/25$). (c) Schematic of the experimental layout with the model centered on top of the shake table platen, whose motion is observed by two cameras procuring high-speed photographs in real time, and additional instrumentation consisting of laser velocimeters and accelerometers. (d) Typical snapshots produced by high-speed photography and digital image correlation. (e) Closeup of laser velocimeters and accelerometers. (f) Accelerometer array on the back of towers at UCB.

Table 1. Details for the ground motion used

Location	Magnitude	Station	Epicenter distance	Fault distance	Peak ground velocity	Peak ground acceleration
Ridgecrest	7.1 Mw	China Lake	5.1 km	3.5 km	0.511 g	42.4 cm/s

fault line. The shake table at Caltech has one-dimensional horizontal capabilities, so we selected the strongest ground motion component (360° channel) for our physical simulation. The one-dimensional shaking was simulated by actuating the shake table platen along the axis parallel to the plane of view of camera A shown in Fig. 4. The velocity record to be input into the shake table controller was scaled according to the scaling relations specified in Eq. (3) and depicted at the bottom of Fig. 2(c). The implication of the scaling is an input velocity record whose speed and time are 1 order of magnitude slower and shorter than in the prototype (real scale). This scaling guarantees similarity between prototype (P) and model (M_1).

A significant challenge was the construction of model towers at different scales. To simulate the layered pattern used in the prototype and furnished by a six-arm crane (Fig. 1), we used a caroussel or stencil with rectangular holes corresponding to the cross-sectional dimensions of the basic blocks (V. Gabuchian, A. Rosakis, J. Harmon, J. Andrade, J. Conte, and J. Restrepo, "Scaled experiments of multiblock tower structures I: Tabletop scale," submitted to Earthquake Eng. Struct. Dyn.). The carrousel effectively furnishes a template that provides the location of each of the 188 unit blocks that constitute a single story in the tower (Fig. 3). Once a story was placed, the carrousel was lifted and then rotated 90° to furnish the template for the next story. This process was repeated 38 times to provide the exact location of each of the $38 \times 188 = 7,144$ blocks in each tower. Both the tiling pattern and juxtaposition of the stories are important to the stability of the tower, as they influence the level of frictional confinement at the top and bottom of each block.

As for the diagnostics, we chose full-field optical methods at this scale for these main reasons: (1) the ability of optical methods to scale up, (2) the ability to take contactless measurements, which was very important to streamline model construction, especially at this scale, and (3) the ability to obtain transient field quantities of interest such as kinematics and deformations. As shown in Fig. 4, two high-speed cameras were placed in front and on top of the tower models. A typical camera view is shown at the bottom left of Fig. 4. We used the method of digital image correlation (Sutton et al. 2009; V. Gabuchian, A. Rosakis, J. Harmon, J. Andrade, J. Conte, and J. Restrepo, "Scaled experiments of multiblock tower structures I: Tabletop scale," submitted to Earthquake Eng. Struct. Dyn.) to convert incremental displacements of the unit blocks into strain fields. In this way, we obtained subblock-resolution kinematic field time histories (displacement, velocity, acceleration) and corresponding strain fields for each model tower. We believe that the use of kinematic and deformation fields for structural mechanics is novel and quite promising, as highlighted in our results. To verify our results, we also deployed three laser velocimeters: one at the platen level, one at the first level, and one at the top of the tower. These velocimeters enabled us to capture the particle velocities of discrete locations (at very high temporal resolution) in the tower specimen as a function of time and compare them to the velocity field evolutions obtained by our full-field optical measurements at those locations.

As we describe in the next subsection, our process is amenable to upscaling, necessitating minimal adaptation and compatibility between scales. In other words, the procedures used to model an MTS at the tabletop scale $\lambda_\ell = 1/107$ are fully compatible and form-identical to the process used to model an MTS at the engineering scale $\lambda_\ell = 1/25$.

Engineering Scale Models ($\lambda_l = 1/25$)

This set of experiments was performed at the UCB Earthquake Simulator Laboratory, currently the largest 6-degree-of-freedom shaking table in the United States. The details of this portion of the physical modeling campaign are specified in an upcoming publication (Restrepo et al., unpublished data, 2021). Fig. 4(b) shows a detailed picture of the experimental layout at this scale. The main dimension of the tower is $\ell^{M_2} = 6.46$ m [Fig. 4(b)], with corresponding block dimensions of $\ell_0^{M_2} = 17$ cm (Fig. 3). The basic blocks are made of concrete, so there is direct material similarity with the prototype, i.e., $\lambda_\mu = 1$. Also, as in the previous subsection, the experiments were conducted at full gravity, i.e., $\lambda_g = 1$. Therefore, once again, the only dimensional scale that has major influence is the length scale $\lambda_\ell = 1/25$.

As in the tabletop experiments, we showcase the results of the concrete tower at engineering scale ($\lambda_\ell = 1/25$) for the 2019 $M_w = 7.1$ Ridgecrest earthquake. We take the same record as before, from a station located 3.5 km away from the fault line. Unlike the Caltech small shake table, the UCB shake table is capable of imposing three-dimensional (3D) translations and rotations. Hence, we simulate the velocity time history in all three displacement axes, as depicted in Fig. 2(b). The 3D shaking was simulated by actuating the shake table platen along the recorded north–south and east–west directions and also in the vertical direction, which corresponds to the longitudinal dimension of the tower [Fig. 2(b)]. Consistent with DMT, the 3D acceleration record input to the shake table controller was scaled according to the relations specified in Eq. (3). There are two major differences with respect to the seismic simulation in the Caltech tabletop experiments. First, even though the input earthquake record is technically the same, the 3D nature of the record at the UC Berkeley shake table is much more realistic than the single-axis input at Caltech. Second, the velocity and time scales used in the engineering scale model (M_2) are about a fifth of those of the prototype (P), in other words, $v^{M_2} \approx 2v^{M_1} \approx 1/5v^P$ and $t^{M_2} \approx 2t^{M_1} \approx 1/5t^P$, as dictated by scaling.

Like the material, geometry, and excitation, the construction process was multiscale, allowing towers to be built using the same general technique relying on a carrousel or stencil. The same pattern of the blocks at each floor was obtained, with 188 blocks per layer (Fig. 3). However, a significant difference from the smaller scale was the need to use a crane to support, lift, rotate, and align the stencil: essential operations to build towers in the specified layered pattern. The layering process was repeated 38 times (number of stories in the tower), with a total of 7,144 concrete blocks per tower. Needless to say, building towers of height equivalent to that of a two-story building is a multiday operation with a dedicated building crew. The specifics of the tower construction at the UCB shake table are provided in an upcoming publication (Restrepo et al., unpublished data, 2021).

Finally, the same optical diagnostics concept was used for the engineering-scale towers: high-speed photography as the basis for digital image correlation to obtain subblock-resolution kinematics. As shown in Fig. 4(b), two cameras were positioned to capture the kinematics of the concrete towers. Camera A was positioned to

observe the front plane of the tower and coaxial with the horizontal velocity $v_1^{M_2}$ and the vertical velocity $v_3^{M_2}$ [Fig. 2(b)]. Camera B was positioned to observe a top plane of the tower and coaxial with the horizontal velocities $v_1^{M_2}$ and $v_2^{M_2}$ [Fig. 2(b)]. To verify the kinematics obtained using optical measurements combined with digital image correlation (DIC), classic accelerometers were installed on the back of the tower as shown in Fig. 4. The array of accelerometers was installed along the center of the tower and was distributed over the height of the tower. The measurements obtained using high-speed photography combined with DIC match the measurements obtained pointwise via velocimeters (in tabletop experiments) and the accelerometer array. This verification provides confidence in our optical measurements, which as indicated before are quite novel to structural diagnostics, especially at the engineering scale. The advantages of optical measurements have been outlined in the previous subsection, but here we should emphasize that scalability is massive at the engineering scale: the effort to set up high-speed cameras and lights is comparable across scales, whereas the installation of analog measurements, such as accelerometers, scales with the number of sensors and the model dimensions.

The physical models at tabletop scale ($\lambda_\ell = 1/107$) and engineering scale ($\lambda_\ell = 1/25$) are similar because of their grounding on DMT, as outlined in (Rosakis et al. 2021). These similar physical models provide a wealth of data showcasing the dynamic behavior of MTS. These data are relevant and invaluable in the validation of numerical (virtual) models, which are presented in the next subsection.

Numerical (Virtual) Modeling

The virtual models in this campaign are needed to show predictive capability to the physical models at both scales. The key to achieving this goal for MTS is in the kinematics of the blocks, not their deformation, so a model that focuses on the efficient modeling of contact and rigid body motion is ideal. Continuum modeling does not achieve this, so we have opted for a discrete approach. With this in mind, LS-DEM was a natural choice as a modeling technique. Discrete element methods rely on the rigid body assumption and Newton's laws to accurately and efficiently model the contact kinetics and individual kinematics of the discrete elements of the system. In this way, key information such as contact forces, frictional dissipation, and the motion of each block over time can be readily and efficiently studied for towers composed of thousands of blocks. The level set variant of DEM is used as a way to define the shape of the blocks without limitations (Kawamoto et al. 2016). Blocks in this study are limited to the simple block shape; however, validating the level set variant now enables the study of more exotic geometries in the future.

In LS-DEM, particle geometry is defined using both level set functions and a set of discrete surface points that work together in a contact algorithm described in full by Kawamoto et al. (2016). Level sets are functions that take a position in space as input, and then output the signed distance of that position to an object surface, where outside an object is positive and inside is negative. Thus if a surface point position for particle i, p_i, gives a negative level set value from the level set of particle j, $\phi_j(x)$, then particle i and j are in contact. The level set value is called the overlap and is denoted d, and the level set also provides the contact normal direction $\hat{n}$ through the gradient

$$\phi_j(\boldsymbol{p}_i) = d \tag{4}$$

$$\frac{\nabla \phi_j(\boldsymbol{p}_i)}{|\nabla \phi_j(\boldsymbol{p}_i)|} = \hat{n} \tag{5}$$

In the bottom right of Fig. 3, a visualization produced from the level set of the representative block is shown with the surface points overlaid.

Once contact is established, the contact forces and the resulting moments are calculated using a contact law. No contact law is specific to the model, and for this study, a linear force–displacement relationship is used for both normal and shear forces. For the linear model, normal and shear forces are written as

$$\boldsymbol{F}_n = k_n d\hat{\boldsymbol{n}} + c\boldsymbol{v}_n^{rel} \tag{6}$$

$$\Delta \boldsymbol{F}_s = k_s \boldsymbol{v}_s^{rel} \Delta t \tag{7}$$

where $\boldsymbol{v}_n^{rel}$ and $\boldsymbol{v}_s^{rel}$ = relative velocity between the contact point on each of two colliding blocks in the normal and shear direction, respectively; Δt = time step; k_n and k_s = normal and shear stiffnesses; and c = contact damping. The contact damping is used to model inelastic contact and is controlled by the nondimensional coefficient of restitution, c_{res}. The shear force uses an incremental approach owing to the history-dependent nature of friction. Coulomb friction is used to model the maximum frictional force as

$$F_s^{\max} = \mu \|\boldsymbol{F}_n\| \tag{8}$$

Moments can then be calculated using the forces and the center of mass of the particle, x_m,

$$M = (\boldsymbol{p}_i - \boldsymbol{x}_m) \times \boldsymbol{F} \tag{9}$$

With the forces and moments from the forces calculated, the motion of the particles can then be determined by Newton's Second Law and kinematics, which results in new contacts, and the process iterates.

The contact algorithm requires certain physical parameters that can all be determined from measurements on individual blocks without the need of tower construction, as reported in Table 2. All parameters in this study were measured at the appropriate scale and for the particular choice of material. It should be noted that parameters could also be determined through scaling, but this method was not pursued in this study. These parameters are common for all applications of DEM except for the application-specific parameter, *block height variation*. This parameter was added after observations from the physical models showed that variation of block heights was causing imperfect stacking arrangements which were believed to affect the dynamics of MTS. The model uses an explicit time integration scheme in which the time step can be set to a known critical time step (Tu and Andrade 2008).

The ground was modeled as a flat plane that develops contact with blocks when a block's surface points cross that plane. Ground motion was modeled by prescribing the motion of the plane. Imposed earthquake ground motion record is often recorded at a different sampling rate than the numerical simulation time step, and therefore linear interpolation was used to up-sample the applied base motion.

Models of the MTS were initialized with each block placed exactly in their designed location in the lateral directions, but in the

Table 2. Complete list of parameters used in numerical modeling

Parameter	Wood	Concrete	Units
Normal stiffness (k_n)	30	1,050	MN/m
Shear stiffness (k_s)	26	1,000	MN/m
Density (ρ)	800	2,320	kg/m³
Friction coefficient (μ)	0.63	0.59	—
Coefficient of restitution (c_{res})	0.3	0.5	—
Block height standard deviation (σ_H)	0.155	0.5	Mm

vertical direction some space was added in between the block layers. The fictitious initial vertical separation is to allow the tower to find equilibrium naturally with gravity and without the interference of initial contact forces. Tower layers were added one at a time, and each layer was lowered at a set velocity to replicate as closely as possible how the tower is built experimentally. This process of the tower settling into static equilibrium was completed before any earthquake ground motion was applied. In cases with significant block height variation, a damping procedure is recommended to achieve the target tower quality and will be discussed in a future paper on the subject.

Results and Model Comparisons

In this section, we showcase the most salient results obtained from the physical models M_1 and M_2 and the virtual models V_1 and V_2. As mentioned earlier, our main objective here is to validate the virtual models using appropriately scaled physical models. Hence, as shown in Figs. 5 and 6, we compare the predictions obtained from V_1 of the response obtained in M_1 at the tabletop scale ($\lambda_\ell = 1/107$), and the predictions obtained from V_2 of the response obtained in M_2 at the engineering scale ($\lambda_\ell = 1/25$). In addition to validating the virtual models against physical models, we also present results related to the validity of the physical models, namely: verify the kinematic fields obtained from the high-speed

cameras and DIC against the independent pointwise measurements obtained using velocimeters and accelerometers; and ascertain the consistency of μ^N and therefore the similarity between models at different scales (e.g., $V_1 \equiv V_2$; $M_1 \equiv M_2$). Hence, we show that (1) our virtual models are valid by comparing them with (2) valid field measurements using DIC, and we show that (3) the whole dynamic modeling approach is consistent.

Fig. 5 shows results comparing the virtual model V_1 with measurements from physical model M_1 at the tabletop scale. The left side of the figure shows comparisons of the v_1 component of velocity at three different time stations, t_1, t_2, and t_3. The component v_1 corresponds to the most significant motion in the models, since in the physical model at $\lambda_\ell = 1/107$, the strong ground motion is aligned with that direction. In fact, the right side panel of Fig. 5 shows the time history of the component v_1 of velocity in the virtual and physical models at various stations along the height of the tower. The time history shown at the bottom corresponds to the motion at the base of the physical model M_1, which was used as input for the virtual model V_1. Before we analyze the results in more detail, it should be remarked that the virtual model V_1 was run 10 times, each time corresponding to a realization of a tower composed of blocks of slightly different heights ℓ_0. The details pertaining to such models will be published in an upcoming paper (Harmon et al., unpublished data, 2021). We chose a normal distribution for the block's height, with a standard deviation of
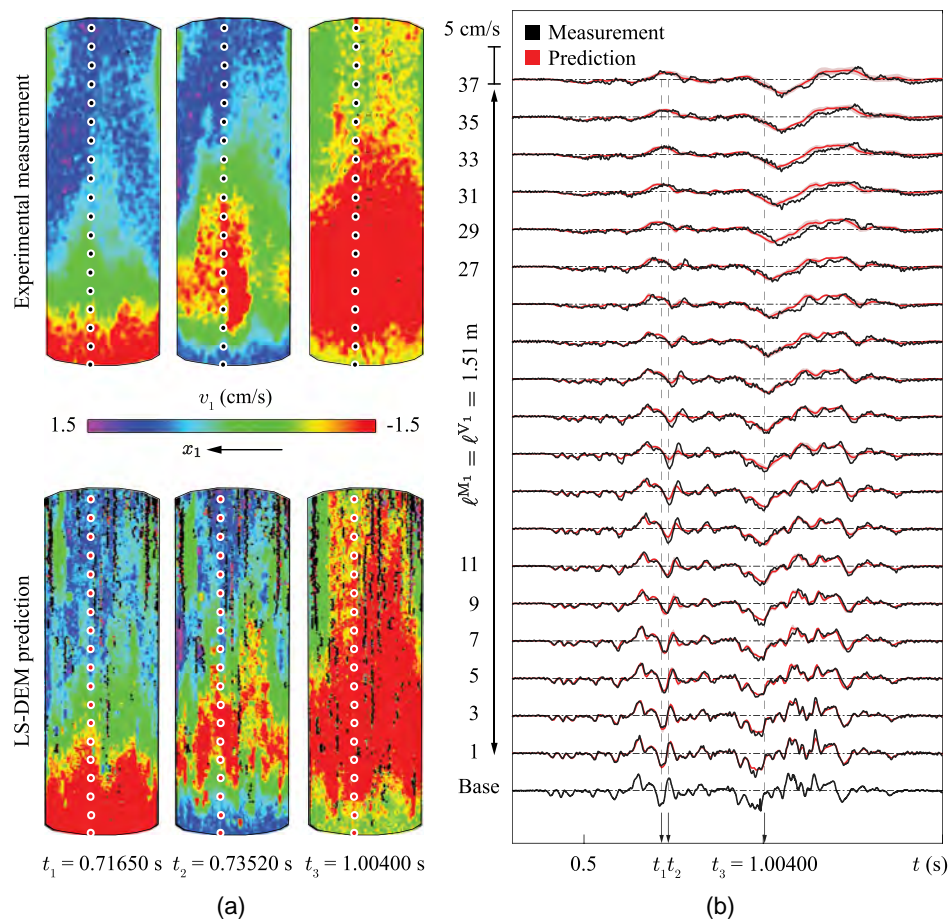
Fig. 5. Overall results and comparisons between physical (M_1) and virtual (V_1) models at $\lambda_\ell = 1/107$ scale: (a) snapshots at three different time stations comparing velocity field v_1 for (top) physical model M_1 with (bottom) virtual model V_1; and (b) velocity v_1 time history for physical model M_1 and virtual model V_1 at different height levels (points sampled in panel a). Shadow band around virtual model predictions V_1 shows spread for 10 different realizations of virtual tower configurations accounting for random block height variability. The line inside the shadow band corresponds to V_1 prediction average.

Fig. 6. Overall results and comparisons between physical (M$_2$) and virtual (V$_2$) models at $\lambda_\ell = 1/25$ scale: (a) snapshots at three different time stations comparing velocity field v_1 for (top) physical model M$_2$ with (bottom) virtual model V$_2$; and (b) velocity v_1 time history for physical model M$_2$ and virtual model V$_2$ at different height levels (points shown on panel a). Shadow band around virtual model predictions V$_1$ shows spread for 10 different realizations of virtual tower configurations accounting for random block height variability. The line inside the shadow band corresponds to V$_2$ prediction average.

0.155 mm (Table 1) obtained from measurements taken from the wood blocks used in the construction of the physical tower at the tabletop scale. Interestingly, without the inclusion of these small imperfections, the virtual model predictions are not as accurate as those obtained using variable block heights. Next, we turn our attention to analyzing the results shown in Fig. 5 both qualitatively and quantitatively.

It is worth noting that the v_1 velocity fields from the experimental and virtual tower specimens in Fig. 5(a) are plotted at the same time stations and using the same intensity map. The qualitative similarity in the velocity fields is strong. Even more remarkable, however, is the quantitative agreement in the details and morphology of the velocity maps. In both models, one can observe a velocity front that moves upwards from the base to the top of the tower at the 38th story. This movement can be observed in both models shown in Fig. 5(a) by looking at the velocity fronts at the three different time stations shown. The timing, location, and morphology of the v_1 velocity fields in both models are in very good agreement, demonstrating the accuracy of the virtual model at this scale ($\lambda_\ell = 1/107$) using wood blocks. Looking more deeply, Fig. 5(b) shows the time history comparisons for v_1 obtained in both models. Unlike the spatially continuous snapshots in time shown on the left panel, the continuous time histories show the evolution of v_1 at discrete locations (red and black points) along the height of the model towers. The agreement between the predictions and measurements is excellent, with the virtual model faithfully capturing

the nonlinear response time history along the height of the tower. In a way, Figs. 5(a and b) offer two sides of the same coin, with panel a offering continuous fields in space but discontinuous snapshots in time, and panel b showing continuous time histories but at discontinuous locations in space. The picture painted by both views is consistent: the virtual model V$_1$ accurately predicts the measured data obtained from the physical model M$_1$.

Fig. 6 shows results for the engineering-scale models ($\lambda_\ell = 1/25$). Once again, the virtual models were run 10 times with variable block heights corresponding to a normal distribution with standard deviation of 0.5 mm (Table 1) obtained from measurements of many concrete blocks in situ. The shaded band in Fig. 6(b) corresponds to the fan of results obtained from the 10 different realizations of the virtual model V$_2$. Accounting for randomly variable height ℓ_0 was crucial for obtaining accurate predictive results, as in the tabletop case. Fig. 6(a) shows comparisons of the velocity v_1 field for both physical model M$_2$ and virtual model V$_2$ at three different time stations, t_1, t_2, and t_3. In contrast to the tabletop experiments, the engineering scale models at $\lambda_\ell = 1/25$ are subjected to 3D input motion at the base [Fig. 2(b)]. Nevertheless, the component v_1 corresponds to the strongest recorded direction of motion and hence presents a relevant component of the velocity field for purposes of model validation. As shown in Fig. 6(a), the velocity fields predicted using the virtual model V$_2$ compare remarkably well to the velocity fields measured from the physical model M$_2$. As in the tabletop models, one can observe a

velocity front whose location, temporal evolution, and shape are similar in both models, whose results are plotted using the same color map. The qualitative and quantitative similarities in the velocity fields is remarkable and complemented by the results showing the velocity time histories.

Fig. 6(b) shows the v_1 velocity time histories for the virtual and physical models at discrete locations along the height of the towers. The v_1 time histories for both V_2 and M_2 compare well, with the salient features in the measured signals being captured by the virtual model. The high- and low-frequency components of response are well predicted, and the peaks and valleys in the time histories correspond to a high degree of accuracy. Figs. 6(a and b) show complementary sides of the measured and predicted responses and indicate a high predictive capability of the virtual model. It is also important to note that there is no deterioration in the predictive power of the virtual model as the length scale is increased; there is also an important level of consistency in the physical models even though the nature of the imposed base excitation differed in dimensionality (1D versus 3D).

This brings us to the issue of consistency. While it is clear that the virtual and physical models are comparable at each scale, i.e., $V_1 \equiv M_1$ and $V_2 \equiv M_2$, it is not clear whether models are consistent across scales, namely $V_1 \equiv V_2$ and $M_1 \equiv M_2$. Consistency requires complete similarity between models and scales, provided the input motions are also similar. In the results presented herein, there is not complete consistency, since the dimensionality of the base excitation is not consistent. However, we did perform simulations using virtual models with consistent excitations and found that these models are fully consistent. Similarly, we performed simulations using physical models that are fully consistent across scales and found that these models are indeed consistent. We present the details of these findings in Rosakis et al. (2021) and Harmon et al. (unpublished data, 2021) but report here that the models are fully consistent due to their appropriate similarity predicated on μ^N.

Finally, we also report on the validity of the optical measurements used in the results provided in Figs. 5 and 6. How do we know that the measured kinematics and subsequently calculated fields using DIC are accurate? To assess this important question, we have to verify the optical measurements using independent measurements and evaluate their consistency. In the case of the results shown in Fig. 5, the optical measurements were compared with velocimeter data (not shown) obtained at the base, bottom, and the top of the tower. In other words, the time history shown for the base, block 1, and block 37 were compared with velocimeter data obtained at those locations. While the data and comparisons will be published in a subsequent publication (V. Gabuchian, A. Rosakis, J. Harmon, J. Andrade, J. Conte, and J. Restrepo, "Scaled experiments of multiblock tower structures I: Tabletop scale," submitted to Earthquake Eng. Struct. Dyn.), we can report that the time histories coincide to within the accuracy of the measurement methods. Hence, the data at $\lambda_\ell = 1/107$ has been validated. We used the same optical technique for the experiments at the engineering scale, $\lambda_\ell = 1/25$. In the case of the engineering-scale measurements, however, we had access to a larger number of locations on the tower where acceleration measurements were taken. As shown in Fig. 4, an array of accelerometers was installed along the height of the tower to provide indirect validation of the optical measurements. The validation is indirect because the accelerometers were placed on the back of the tower, whereas the optical measurements were taken on the front of the tower. However, there is a relatively high degree of symmetry in the problem (especially early on during the seismic tests) and hence comparisons can be made. We report the data and comparisons of the optical and accelerometer data in an upcoming publication (Restrepo et al., unpublished data, 2021). We also report here that the optical and accelerometer data obtained

are in very good agreement. Also, the velocities obtained at the base of the tower were compared with those reported by the control system of the shake table at UCB, and they match reasonably well. A number of independent measurements coincide in space and time with the optical measurements; we therefore conclude that the optical measurements are valid across scales.

Closure

We have presented a systematic methodology to assess the seismic performance of a new type of MTS designed to serve as a gravitational energy storage system. These MTS possess great potential as energy storage systems at a moment when there is much interest and need to expand energy storage capacity worldwide. The discontinuous nature of the MTS systems pose a number of challenging and interesting engineering questions, particularly, how can we model such discontinuous gravitational-frictional systems? This paper summarizes a year-long integrated theoretical-numerical-experimental campaign to begin answering the question of modeling such systems. The presentation is rather superficial and incomplete due to the nature of this introductory paper. However, we have reported on a number of important findings that will be expanded in a number of companion publications (Rosakis et al. 2021; Harmon et al., unpublished data, 2021; V. Gabuchian, A. Rosakis, J. Harmon, J. Andrade, J. Conte, and J. Restrepo, "Scaled experiments of multiblock tower structures I: Tabletop scale," submitted to Earthquake Eng. Struct. Dyn.; Restrepo et al., unpublished data, 2021). In particular, we have shown the process by which we have constructed similar models of MTS across scales $\lambda_\ell = 1/107$ and $\lambda_\ell = 1/25$ and used them to validate virtual numerical models using LS-DEM. The central piece to achieving similar physical models is the nondimensional number μ^N, which seems to control gravitational-frictional systems. This new nondimensional number expands the toolbox of experimental dynamic modelers used to continuum classic numbers such as Cauchy and Froude, useful in modeling elastic and frictionless-gravitational systems, respectively, in engineering.

Appropriate scaling enabled us to successfully design, build, and diagnose MTS under dynamic loading. We used the same methodology regardless of scale, particularly in construction and diagnostics. The diagnostics deployed a novel and scalable concept of optical measurements hinging on high-speed photography enhanced with DIC. This enabled the measurement of kinematic fields at subblock resolution, furnishing spatiotemporal fields for displacement, velocity, and acceleration. The optical measurements were properly validated using a number of independent measurements across material, length, and time scales.

The main objective of the study was to validate computational (virtual) models of MTS that are predicated on Newtonian mechanics, a significantly different framework from finite element modeling, which is rooted in continuum mechanics. Our discontinuous approach uses basic physics and contact-frictional mechanics to model MTS as a collection of rigid blocks that interact with each other, being controlled by Newton's Second Law and modulated by contact-frictional mechanics. This simple physics-based approach was shown to be predictive in space and time, regardless of length scaling. Strong similarities in fields and time histories of velocity components were shown as salient examples of a wealth of results that will be reported subsequently.

The results presented in this paper show that discrete models, such as LS-DEM, can be appropriately used to simulate the behavior of complex MTS. We have also shown that dynamic modeling theory provides the tools to construct and test similar physical

models of MTS. Equipped with these predictive and validated modeling tools, one can perform analysis of MTS for a broad range of expected seismic loads across the globe. It is anticipated that such an approach can be used to design future MTS systems and, eventually, assess the seismic performance of these novel gravity energy storage systems.

Appendix. Block Rotation Data

To evaluate whether this system is one featuring primarily sliding blocks or whether the rotations (and rotation rates) are big enough to activate additional interfacial forces comparable to pure gravity, the in-plane rotations (rotations about the tower-camera axis) of the blocks were measured using DIC. Fig. 7 shows the time histories of the centroidal rotations through the entire duration of the excitation reported in an inertial frame. For simplicity, we highlight the maximum values, θ_{max}, of $\theta(t)$ at each level.

What is remarkable about this figure is that the maximum value, θ_{max}, of these angles ranges between 0.05° and 0.18°, indicating that the individual blocks, at all levels and at all times, feature minimal rocking and slide rocking response. This measurement provides ample justification for the use of μ^N scaling, since the system is clearly dominated by sliding across horizontal interfaces.
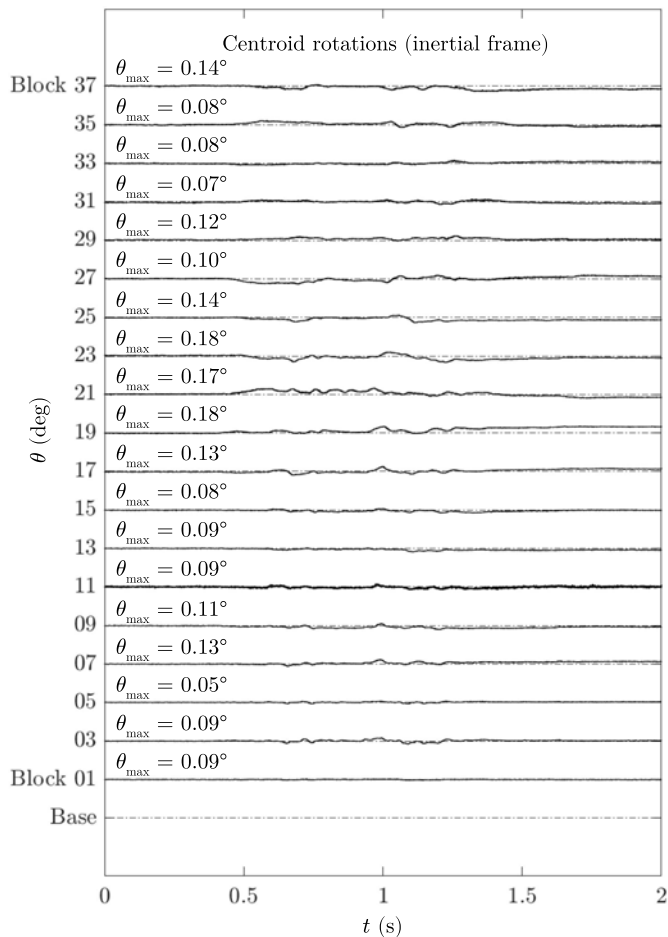
Fig. 7. Ridgecrest ground motion on the wood tower constructed at Caltech (M_1) caused minimal rotations about the tower-camera axis as captured by DIC. These results are shown as an example, as other towers showed similar rotations. The maximum rotation for each block of the spine is shown above the line. Such low rotations imply that the motion of the blocks is largely due to sliding.

Numerically we can verify that rocking rotations in both the x and y axis were also minimal or nonexistent.

Data Availability Statement

All data, models, or code that support the findings of this study are available from the corresponding author upon reasonable request.

References

Buckingham, E. 1914. "On physically similar systems: Illustration of the use of dimensional equations." *Phys. Rev.* 4 (4): 345–376. https://doi.org/10.1103/PhysRev.4.345.

EIA (US Energy Information Administration). 2020. *Electricity explained: Electricity generation, capacity, and sales in the United States.* Washington, DC: US Energy Information Administration.

Energy Efficiency and Renewable Energy. 2021. *Pumped storage hydropower.* Washington, DC: DOE.

Harris, H., and G. Sabnis. 1999. *Structural modeling and experimental techniques.* Boca Raton, FL: CRC Press.

Henze, V. 2018. *Energy storage is a $620 billion investment opportunity to 2040.* New York: BloombergNEF.

IEA (Internal Energy Agency). 2017. "Energy storage tracking clean energy process." Accessed January 25, 2021. https://www.iea.org/reports/tracking-clean-energy-progress-2017.

Janney, J., J. Breen, and H. Geymayer. 1970. "Use of models in structural engineering." In *Models for concrete structures*, 1–18. Detroit: American Concrete Institute.

Kawamoto, R., E. Ando, G. Viggiani, and J. Andrade. 2016. "Level set discrete element method for three-dimensional computations with triaxial case study." *J. Mech. Phys. Solids* 91 (4): 1–13. https://doi.org/10.1016/j.jmps.2016.02.021.

Loveless, M. 2012. "Energy storage: The key to a reliable, clean electricity supply." Accessed January 25, 1994. https://www.energy.gov/articles/energy-storage-key-reliable-clean-electricity-supply.

Markolf, S., I. Azevedo, M. Muro, and D. Victor. 2020. *Pledges and progress: Steps toward greenhouse gas emissions reductions in the 100 largest cities across the United States.* Washington, DC: Brookings Institute.

Moncarz, P., and H. Krawinkler. 1981. *Theory and applications of experimental model analysis in earthquake engineering.* Stanford, CA: Stanford Univ.

Rosakis, A., J. Andrade, V. Gabuchian, J. Harmon, J. Conte, and J. Restrepo. 2021. "Implications of Buckingham's Pi Theorem to the study of similitude in discrete structures: Introduction of the R_F^N, μ^N, and the S^N dimensionless numbers and the concept of structural speed." *J. Appl. Mech.* 88 (9): 091008. https://doi.org/10.1115/1.4051338.

Sutton, M. A., J. J. Orteu, and H. Schreier. 2009. *Image correlation for shape, motion and deformation measurements: Basic concepts, theory and applications.* Berlin: Springer.

Tu, X., and J. E. Andrade. 2008. "Criteria for static equilibrium in particulate mechanics computations." *Int. J. Numer. Methods Eng.* 75 (13): 1581–1606. https://doi.org/10.1002/nme.2322.

UN (United Nations). 2019. *World population prospects 2019: Highlights.* New York: United Nations, Department of Economic and Social Affairs.

Zablocki, A. 2019. "Fact sheet: Energy storage." Accessed January 25, 1994. https://www.eesi.org/papers/view/energy-storage-2019.